

Identification of acoustically induced spin resonances of Si vacancy centers in 4H-SiC

T. Vasselon,¹ A. Hernández-Mínguez,² M. Hollenbach,^{3,4} G. V. Astakhov,³ and P. V. Santos²

¹*Université Grenoble Alpes, CNRS, Grenoble INP, Institut Néel, 38000 Grenoble, France*

²*Paul-Drude-Institut für Festkörperelektronik, Leibniz-Institut im Forschungsverbund Berlin e.V.,*

Hausvogteiplatz 5-7, 10117 Berlin, Germany

³*Helmholtz-Zentrum Dresden-Rossendorf, Institute of Ion Beam Physics and Materials Research, Bautzner Landstrasse 400, 01328 Dresden, Germany*

⁴*Technische Universität Dresden, 01062 Dresden, Germany*

(*alberto.h.minguez@pdi-berlin.de)

(Dated: December 16, 2022)

Silicon vacancies (V_{Si}) in the 4H polytype of SiC form color centers with long-lived and optically addressable spin states, which make them promising spin qubits for quantum communication and sensing. These centers can be created both in the cubic ($V2$) and in the hexagonal ($V1$) local crystallographic environments of the 4H-SiC host. While the $V2$ center can be efficiently manipulated by optically detected magnetic resonance (ODMR) even at room temperature, ODMR control of the $V1$ centers could so far only been achieved at cryogenic temperatures. Here, we show that magnetic resonance induced by the dynamic strain of a surface acoustic wave can overcome this limitation and enable the efficient manipulation of $V1$ centers up to room temperatures. Based on the width and temperature dependence of the acoustically induced spin resonances, we attribute them to spin transitions between the $+3/2$ and $-1/2$ spin sublevels of the excited state of the $V1$ centers. These results are an important step towards on-chip quantum information processing based on V_{Si} centers driven by acoustic fields.

Atom-like color centers in SiC are attractive systems for applications in quantum communication and sensing [1–6]. The most prominent example is the negatively charged silicon vacancy (V_{Si}) [7]. This center emits in the near infrared range, where optical glass fibers have low absorption, and it has long-living spin states, which can be optically addressed and controlled by microwave (MW) fields even at room temperature [8–10]. Similar to an oscillating magnetic field, elastic vibrations can also induce room-temperature interlevel spin transitions in such center [11]. In contrast to MW-induced spin resonances, which only allow changes in spin number $\Delta m_S = \pm 1$ [12], acoustic fields can also induce spin transitions with $\Delta m_S = \pm 2$ both in the ground and excited state multiplets [13], thus opening new ways for the on-chip coherent manipulation of individual spin qubits with coherent acoustic fields.

Silicon atoms in the 4H-SiC polytype occupy two non-equivalent sites with the hexagonal (h) and cubic (k) crystallographic local environments illustrated in Fig. 1(a). Vacancies at these sites create two types of V_{Si} centers labeled as $V1$ and $V2$, respectively [14]. Both types share the same half-integer spin $S = 3/2$, but their orbital and spin transitions have different energies due to the non-common local environments [14]. The $V2$ center has been intensively studied due to its long spin coherence time even at room temperature and the fact that it can be addressed using conventional optically detected magnetic resonance (ODMR) [15–21]. In contrast, only a few investigations have focused on the $V1$ center, where spin control by optically detected methods has only been reported at cryogenic temperatures [22, 23]. However, the $V1$ center is also a promising quantum system for the realization of robust spin-photon interfaces [22, 24, 25], provided that an efficient method for its spin manipulation and readout is demonstrated. In this manuscript, we employ acoustic vibrations in the form of surface acoustic waves (SAWs) to efficiently induce spin transitions in both the $V1$ and $V2$ centers. By employing a

spectrally filtered ODMR technique, we unveil acoustically induced spin transitions in the $V1$ center up to room temperature and discriminate them from the spin transitions of the $V2$ center.

Figure 1(b) displays the hybrid spin-optomechanical system used in this work. The device consists of a 4H-SiC substrate containing an ensemble of V_{Si} centers created at a depth of $2.5 \mu\text{m}$ by proton irradiation with an energy of 375 keV and a fluence of 10^{15} cm^{-2} . For SAW excitation, the SiC substrate was coated with a 700-nm-thick piezoelectric ZnO film, and an acoustic cavity consisting of two focusing interdigital transducers (IDTs) was patterned by electron beam lithography and lift-off metallization. The IDTs excite SAWs with a wavelength $\lambda_{\text{SAW}} = 6 \mu\text{m}$ and a frequency $f_{\text{SAW}} \approx 920 \text{ MHz}$. The experiments were performed in a confocal microphotoluminescence ($\mu\text{-PL}$) setup with the sample placed in a cold-finger cryostat equipped with a window for optical access and radio-frequency connections for the application of MW signals to the IDTs. The V_{Si} centers were optically excited using a 780 nm laser beam focused on a spot with diameter of $10 \mu\text{m}$ by a 20x objective with 0.4 numerical aperture. The PL from the centers was collected by the same objective, the laser stray light was removed using a long-pass dichroic mirror (805 nm), and then the PL spectrum was analyzed by a monochromator equipped with a charge-coupled device camera. Figure 1(c) shows the PL spectrum of the V_{Si} centers measured at 20 K. Three zero-phonon lines (ZPLs) are observed at 858 nm ($V1'$), 862 nm ($V1$) and 917 nm ($V2$) superimposed on their corresponding broad phonon sidebands (PSBs) [22]. The $V1$ and $V2$ lines are the optical transitions between the ground state (GS) and the first excited state (ES) of the centers, while the $V1'$ line is the optical transition between the GS and the second ES of the $V1$ center. At room temperature, the PL is dominated by the broad emission from phonon induced sidebands, and the ZPLs are no longer observed, see Fig. 1(d).

The acoustically induced ODMR (aODMR) studies were

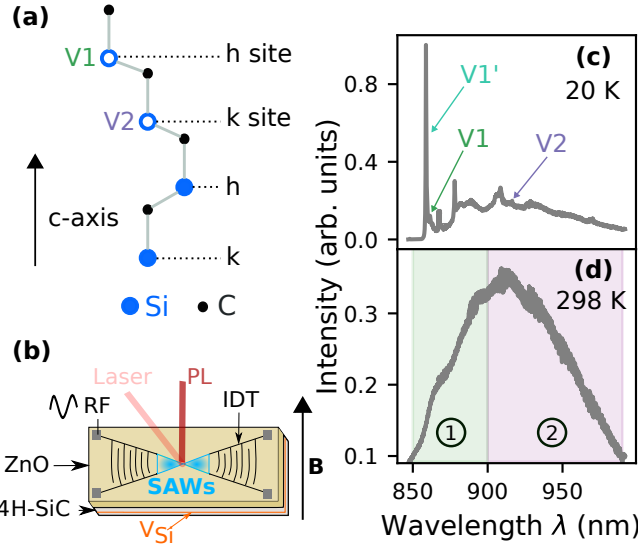


FIG. 1. (a) Schema of the two non-equivalent sites for the silicon atom (the h and k sites) in 4H-SiC, which correspond to the V1 and the V2 centers. (b) Sketch of the acousto-electric device. It consists of a 4H-SiC wafer containing V_{Si} centers at a well defined depth and coated with a ZnO thin film. An acoustic cavity consisting of two focusing IDTs is patterned on the ZnO film to excite SAWs. (c) Photoluminescence spectrum of the 4H-SiC at 20 K. (d) Same as (c), but measured at room temperature. The areas marked as 1 and 2 indicate the PL spectral regions used in the aODMR experiments.

performed by detecting the PL integrated over the phonon sidebands using a silicon photodiode and several sets of long- and short-pass optical filters. To analyze the aODMR of the V1 centers, we collected the photons emitted in the 850-900 nm spectral region, while for the V2 centers the photodiode detected the PL emitted above 900 nm, see the green and purple regions marked as 1 and 2 in Fig. 1(d), respectively. In both cases, the MW signal applied to the IDTs was amplitude-modulated and the output signal of the photodiode was locked-in to the modulation frequency. To tune the spin transitions in the V_{Si} centers to the SAW frequency, an electromagnet induced a magnetic field $\mathbf{B} = (0, B, 0)$ along the surface direction perpendicular to the SAW propagation, see Fig. 1(b). Under these experimental conditions, the rate for SAW-induced spin transitions with $\Delta m_S = \pm 2$ is maximum, but is zero for the $\Delta m_S = \pm 1$ ones [11]. The spin Hamiltonian for the GS and ES of the V_{Si} centers in the uniaxial approximation is [26]:

$$\mathcal{H}_0^{(GS,ES)} = D^{(GS,ES)} (S_z^2 - \frac{5}{4}) + g\mu_B B S_y, \quad (1)$$

where $g \approx 2$ is the Landé g -factor, μ_B the Bohr magneton, \mathbf{S} the $3/2$ -spin operator with S_z its component parallel to the crystallographic c axis [see Fig. 1(a)], and $D^{(GS,ES)}$ are the zero field splitting (ZFS) constants. Under zero magnetic field, the spin sublevels in the GS and ES are split into two Kramer's doublets along the z direction. The splitting amplitudes of the V1 center have so far only been reported for cryogenic temperatures with values $2D^{(GS)} = 4$ MHz and

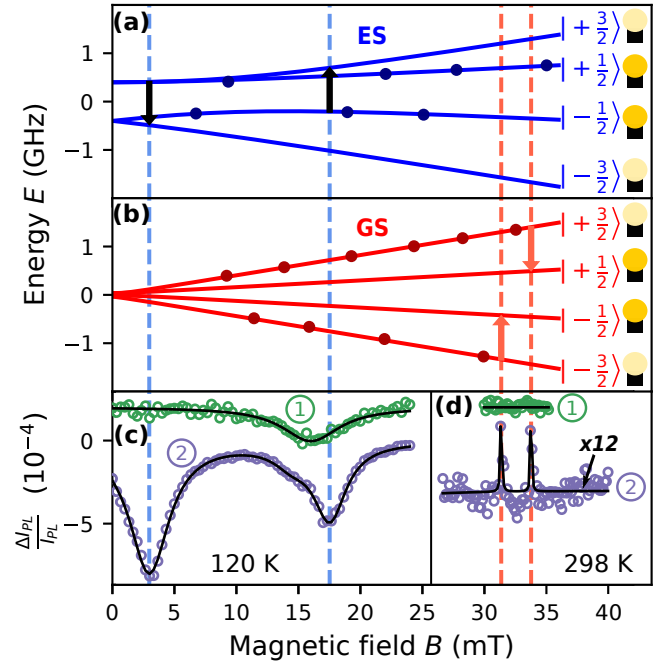


FIG. 2. (a) and (b) are the magnetic field dependence of the ES and GS spin sublevels, respectively, for the V2 centers. The red and blue dots indicate the preferentially populated states under optical excitation. The PL intensity is stronger for optical transitions between the ES and GS in the $m_S = \pm 1/2$ spin states, (see on/off bulbs next to each spin sublevel). The red (GS) and blue (ES) dashed lines indicate expected magnetic fields for spin resonances under $f_{SAW} = 921$ MHz (see magnitude of the vertical arrows). (c) Acoustically induced ODMR measurements as a function of magnetic field for $\Delta m_S = \pm 2$ spin transitions. The green and purple circles are measurements collecting photons in the spectral regions 1 and 2, respectively. The black curves are a multi-peak fitting of the experimental data using Lorentzian functions. (d) Same as (c), but for MW-induced $\Delta m_S = \pm 1$ resonances.

$2D^{(ES)} = 985$ MHz [23]. In contrast, the ZFSs for the V2 center have been measured for a wide range of temperatures: the splitting in the GS is almost temperature independent with $2D^{(GS)} = 70$ MHz, while in the ES it is $2D^{(ES)} = 430$ MHz at room temperature and increases linearly with decreasing temperature up to $2D^{(ES)} = 1050$ MHz at 4 K [27]. Under strong magnetic field, the Zeeman term in the spin Hamiltonian splits all sublevels and the spin projection becomes quantized along y .

Figures 2(a) and (b) display the expected dependence of the ES and GS spin sublevels for the V2 center under the in-plane magnetic field. The optical transitions between the GS and ES are spin-conserving. However, optical excitation followed by non-radiative spin-selective intersystem crossing via metastable states lead to a preferential population of the $m_S = \pm 1/2$ states in the ES (blue dots) and the $m_S = \pm 3/2$ states in the GS (red dots), as well as a stronger PL intensity for optical transitions between the GS and ES with $m_S = \pm 1/2$ states than with $m_S = \pm 3/2$ [see light bulbs in Figs. 2(a) and (b)] [13]. Figures 2(c) and (d) show acoustically and MW-induced ODMR measurements acquired in the magnetic field

ranges expected for $\Delta m_S = \pm 2$ and $\Delta m_S = \pm 1$ spin transitions, respectively. At high magnetic fields (above 25 mT), we observe two narrow peaks corresponding to the $\Delta m_S = \pm 1$ spin transitions between the $m_S = \pm 3/2$ and $m_S = \pm 1/2$ sublevels in the GS of the V2 centers, see purple circles in Fig. 2(d) and red vertical arrows in Fig. 2(b). Such resonances are not excited in aODMR experiments under in-plane **B** perpendicular to the SAW propagation direction [11], but they are driven by the MW magnetic field applied to the IDTs [13]. As expected, no MW-induced ODMR signal is observed for the V1 centers at room temperature, see green circles in Fig. 2(d).

The situation is different for measurements at low magnetic fields (below 25 mT). Here, the aODMR signal for the PL emitted above 900 nm (purple circles) also shows two resonances, but in this case they are two broad dips corresponding to the $+1/2 \rightarrow -3/2$ and $-1/2 \rightarrow +3/2$ spin transitions in the ES of the V2 center [see black vertical arrows in Fig. 2(a)]. Their broadening with respect to the GS resonances arises from the short lifetime of the centers at the ES. These $\Delta m_S = \pm 2$ spin transitions are typically forbidden in MW-induced ODMR experiments, and their observation is a prove that they are excited by the dynamic strain field of the SAWs. In contrast, the aODMR measurement in the 850-900 nm spectral region (open green circles) only shows a broad dip at a magnetic field position that differs from the ones observed for the V2 centers. Therefore, we attribute this resonance to an acoustically induced spin transition in the V1 centers.

To better understand the nature of this V1 spin resonance, we repeated the measurement at several temperatures and fitted the experimental data with Lorentzian functions. Figure 3 shows the results for four different temperatures. In all cases, the aODMR measurement in the 850-900 nm spectral region (green circles) showed the single broad dip attributed to the V1 centers. Its amplitude is approximately temperature independent, but it shifts its position from 17 mT to 15 mT as the temperature goes down. In contrast, the number of peaks and dips observed for the PL emitted above 900 nm (purple circles) depends on temperature. At high temperatures, we observe the broad resonances of the ES together with narrow resonances around 16 mT corresponding to the $\Delta m_S = \pm 2$ GS spin transitions in the V2 centers, as have been described in our earlier work [13]. In addition, the broad dip attributed to the V1 centers is also partially observed due to the fact that a fraction of the Stokes PSB of the V1 center extends beyond 900 nm. Conversely, photons from the anti-Stokes PSB of the V2 centers emitting within the 850-900 nm range make the aODMR measurements in this spectral region partially sensitive to the resonances of the V2 center (see weak dips around 10 mT for 298 K and 220 K). As the temperature decreases, the reduction in the PSB emission suppresses this cross-detection effect. Moreover, the narrow GS spin transitions cannot be resolved at temperatures below 200 K due to the large amplitude of the ES spin resonances in the V2 center at this temperature range.

Figure 4 summarizes all identified spin resonances for different temperatures. The solid red triangles and blue circles are the results of the Lorentzian fits in Fig. 3 for the GS and ES spin sublevels of the V2 centers, respectively. The

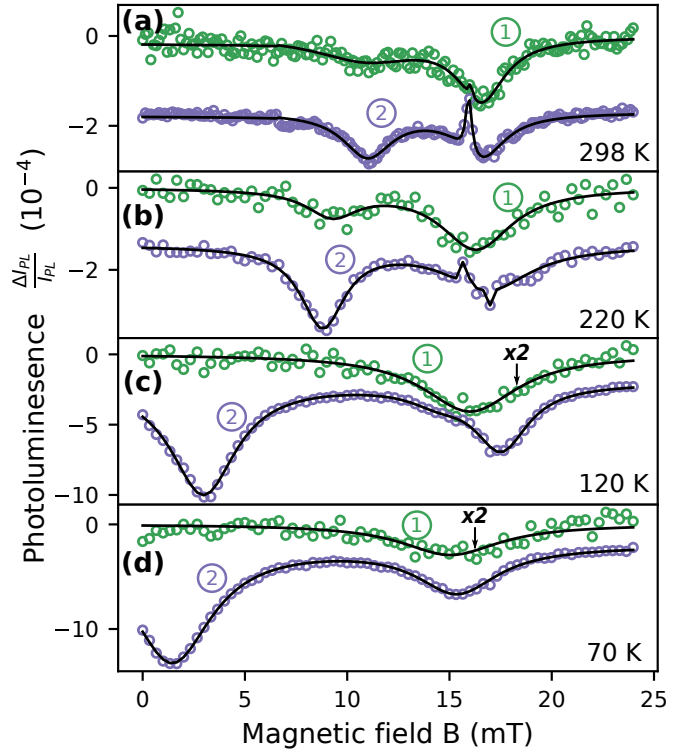


FIG. 3. aODMR measurements at (a) 298 K, (b) 220 K, (c) 120 K and (d) 70 K, obtained by collecting the PL emitted in the spectral region 1 (green circles) and 2 (purple circles). The black curves are multi-peak fittings of the experimental data using Lorentzian functions. The aODMR measurements are vertically shifted for clarity.

red dotted and blue dashed curves represent the theoretical dependencies calculated using Eq. 1 and taking into account the temperature dependencies of $2D^{(GS)}$ and $2D^{(ES)}$ [27]. The open green squares are the fitted positions of the measured spin resonances corresponding to the V1 center.

We now discuss the origin of the V1 resonance. In the absence of ZFS, the Zeeman splitting between spin sublevels induced by the in-plane magnetic field causes the frequency of both $\Delta m_S = \pm 2$ spin transitions to match the SAW frequency at the same magnetic field $B = h f_{\text{SAW}} / (g \mu_B \Delta m_S) = 16.5$ mT. This value agrees well with the room temperature position of the V1 resonance and suggests that it could correspond to a GS spin transition, because $2D^{(GS)} = 4$ MHz for the V1 center [23] (we suppose here a temperature independent ZFS for the GS of the V1 center as in the case of the V2 center) and therefore its contribution to the spin Hamiltonian can be neglected.

However, due to the fact that the spin centers stay longer time in the GS than in the ES, GS spin transitions are typically characterized by narrow resonances and ES spin transitions by broad ones, as can be seen in the ODMR signal of the V2 centers in Figs. 2 and 3. The width of the V1 resonance is comparable to the width of the ES resonances of the V2 center, thus suggesting that the V1 resonance should rather be associated to an ES spin transition than to a GS one. Moreover, the V1 resonance shifts to lower magnetic fields at

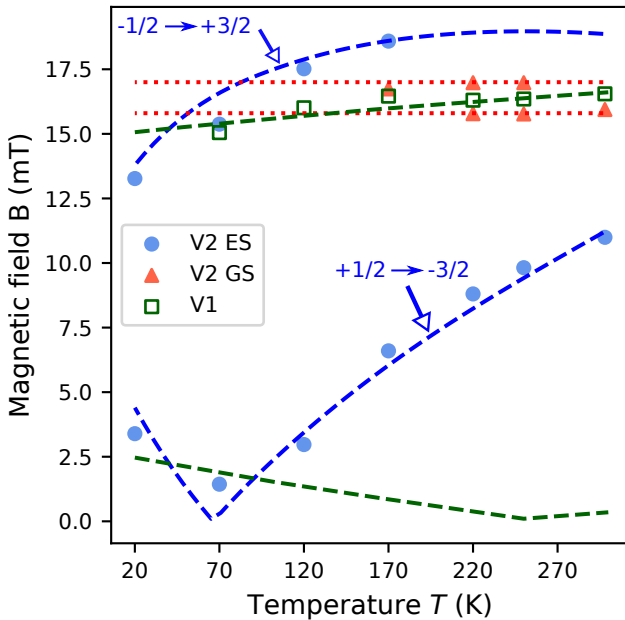


FIG. 4. Temperature dependence of the magnetic field position of the spin transitions. The full circles and triangles are the measured positions of the spin resonances in the ES and GS, respectively, for the V2 centers. The open green squares are the measured positions of the V1 spin transitions. The dotted and dashed lines are the theoretical calculations.

low temperatures, following a similar behavior as for the spin transition between the ES $m_S = +3/2$ and $m_S = -1/2$ spin sublevels in the V2 center, although with a weaker temperature dependence. To study this possibility in more detail, we have calculated the temperature dependence of the $\Delta m_S = \pm 2$ ES spin transitions supposing that the ZFS shifts linearly from $2D^{(ES)} = 985$ MHz at 4 K [23] to $2D^{(ES)} = 920$ MHz at 300 K. The green dashed curves in Fig. 4 show the result of our calcu-

lation. The experimental data agree well with the theoretical values for the spin transition between the ES $m_S = +3/2$ and $m_S = -1/2$ spin sublevels. However, the theory also predicts a spin resonance at low magnetic fields (below 3 mT) which we were not able to detect in our experiments. A possible reason for the absence of this resonance could be that its strength is too low to be resolved in our experimental system.

In summary and conclusion, we have demonstrated acoustically induced spin transitions both in the V1 and V2 centers in 4H-SiC. In contrast to MW-induced spin resonances, which for the V1 centers have only been observed at cryogenic temperatures, the SAW-induced spin resonances are observed for all temperatures studied, even at room temperature. Based on the width of the V1 resonance and its shifting to lower magnetic fields as the temperature decreases, we attribute it to spin transitions between spin sublevels in the excited state. Although a more comprehensive understanding of the acoustically induced spin resonances in V1 centers will require additional studies that go beyond the scope of this manuscript, the demonstration of SAW induced spin resonances in both the V1 and V2 centers at room temperature is an important step toward on-chip quantum information processing based on V_{Si} spins driven by acoustic fields.

ACKNOWLEDGMENTS

The authors would like to thank S. Meister and S. Rauwerdink for technical support in the preparation of the sample, and O. Brandt for a critical reading of the manuscript. G. V. A. acknowledges the support from the German Research Foundation (DFG) under Grant No. AS 310/9-1. The authors acknowledge support from the Ion Beam Center (IBC) at Helmholtz-Zentrum Dresden-Rossendorf (HZDR) for the proton irradiation.

[1] S. Castelletto, B. C. Johnson, and A. Boretti, Quantum Effects in Silicon Carbide Hold Promise for Novel Integrated Devices and Sensors, *Adv. Opt. Mater.* **1**, 609 (2013).

[2] H. Kraus, V. A. Soltamov, F. Fuchs, D. Simin, A. Sperlich, P. G. Baranov, G. V. Astakhov, and V. Dyakonov, Magnetic field and temperature sensing with atomic-scale spin defects in silicon carbide, *Sci. Rep.* **4**, 5303 (2014).

[3] W. F. Koehl, H. Seo, G. Galli, and D. D. Awschalom, Designing defect spins for wafer-scale quantum technologies, *MRS Bull.* **40**, 1146 (2015).

[4] M. Radulaski, M. Widmann, M. Niethammer, J. L. Zhang, S.-Y. Lee, T. Rendler, K. G. Lagoudakis, N. T. Son, E. Janzén, T. Ohshima, J. Wrachtrup, and J. Vučković, Scalable Quantum Photonics with Single Color Centers in Silicon Carbide, *Nano Lett.* **17**, 1782 (2017).

[5] D. D. Awschalom, R. Hanson, J. Wrachtrup, and B. B. Zhou, Quantum technologies with optically interfaced solid-state spins, *Nat. Photonics* **12**, 516 (2018).

[6] M. Atatüre, D. Englund, N. Vamivakas, S.-Y. Lee, and J. Wrachtrup, Material platforms for spin-based photonic quantum technologies, *Nat. Rev. Mater.* **3**, 38 (2018).

[7] E. Janzén, A. Gali, P. Carlsson, A. Gällström, B. Magnusson, and N. T. Son, The silicon vacancy in SiC, *Physica B Condens. Matter* **404**, 4354 (2009).

[8] W. F. Koehl, B. B. Buckley, F. J. Heremans, G. Calusine, and D. D. Awschalom, Room temperature coherent control of defect spin qubits in silicon carbide, *Nature* **479**, 84 (2011).

[9] P. G. Baranov, A. P. Bundakova, A. A. Soltamova, S. B. Orlinskii, I. V. Borovykh, R. Zondervan, R. Verberk, and J. Schmidt, Silicon vacancy in SiC as a promising quantum system for single-defect and single-photon spectroscopy, *Phys. Rev. B* **83**, 125203 (2011).

[10] D. Riedel, F. Fuchs, H. Kraus, S. Väth, A. Sperlich, V. Dyakonov, A. A. Soltamova, P. G. Baranov, V. A. Ilyin, and G. V. Astakhov, Resonant Addressing and Manipulation of Silicon Vacancy Qubits in Silicon Carbide, *Phys. Rev. Lett.* **109**, 226402 (2012).

[11] A. Hernández-Mínguez, A. V. Poshakinskiy, M. Hollenbach, P. V. Santos, and G. V. Astakhov, Anisotropic Spin-Acoustic Resonance in Silicon Carbide at Room Temperature, *Phys. Rev.*

Lett. **125**, 107702 (2020).

[12] S. A. Tarasenko, A. V. Poshakinskiy, D. Simin, V. A. Soltamov, E. N. Mokhov, P. G. Baranov, V. Dyakonov, and G. V. Astakhov, Spin and Optical Properties of Silicon Vacancies in Silicon Carbide - A Review, *Phys. Status Solidi B* **255**, 1700258 (2018).

[13] A. Hernández-Mínguez, A. V. Poshakinskiy, M. Hollenbach, P. V. Santos, and G. V. Astakhov, Acoustically induced coherent spin trapping, *Sci. Adv.* **7**, eabj5030 (2021).

[14] V. Ivády, J. Davidsson, N. T. Son, T. Ohshima, I. A. Abrikosov, and A. Gali, Identification of Si-vacancy related room-temperature qubits in 4H silicon carbide, *Phys. Rev. B* **96**, 161114(R) (2017).

[15] V. A. Soltamov, A. A. Soltamova, P. G. Baranov, and I. I. Proskuryakov, Room Temperature Coherent Spin Alignment of Silicon Vacancies in 4H- and 6H-SiC, *Phys. Rev. Lett.* **108**, 226402 (2012).

[16] H. Kraus, V. A. Soltamov, D. Riedel, S. Väth, F. Fuchs, A. Sperlich, P. G. Baranov, V. Dyakonov, and G. V. Astakhov, Room-temperature quantum microwave emitters based on spin defects in silicon carbide, *Nat. Phys.* **10**, 157 (2014).

[17] M. Widmann, S.-Y. Lee, T. Rendler, N. T. Son, H. Fedder, S. Paik, L.-P. Yang, N. Zhao, S. Yang, I. Booker, A. Denisenko, M. Jamali, S. A. Momenzadeh, I. Gerhardt, T. Ohshima, A. Gali, E. Janzén, and J. Wrachtrup, Coherent control of single spins in silicon carbide at room temperature, *Nat. Mater.* **14**, 164 (2015).

[18] S. G. Carter, Ö. O. Soykal, P. Dev, S. E. Economou, and E. R. Glaser, Spin coherence and echo modulation of the silicon vacancy in 4H-SiC at room temperature, *Phys. Rev. B* **92**, 161202(R) (2015).

[19] M. Niethammer, M. Widmann, S.-Y. Lee, P. Stenberg, O. Kordina, T. Ohshima, N. T. Son, E. Janzén, and J. Wrachtrup, Vector Magnetometry Using Silicon Vacancies in 4H-SiC Under Ambient Conditions, *Phys. Rev. Appl.* **6**, 034001 (2016).

[20] D. Simin, H. Kraus, A. Sperlich, T. Ohshima, G. V. Astakhov, and V. Dyakonov, Locking of electron spin coherence above 20 ms in natural silicon carbide, *Phys. Rev. B* **95**, 161201(R) (2017).

[21] J. S. Embley, J. S. Colton, K. G. Miller, M. A. Morris, M. Meehan, S. L. Crossen, B. D. Weaver, E. R. Glaser, and S. G. Carter, Electron spin coherence of silicon vacancies in proton-irradiated 4H-SiC, *Phys. Rev. B* **95**, 045206 (2017).

[22] R. Nagy, M. Widmann, M. Niethammer, D. B. R. Dasari, I. Gerhardt, Ö. O. Soykal, M. Radulaski, T. Ohshima, J. Vučković, N. T. Son, I. G. Ivanov, S. E. Economou, C. Bonato, S.-Y. Lee, and J. Wrachtrup, Quantum Properties of Dichroic Silicon Vacancies in Silicon Carbide, *Phys. Rev. Appl.* **9**, 034022 (2018).

[23] R. Nagy, M. Niethammer, M. Widmann, Y.-C. Chen, P. Udvarhelyi, C. Bonato, J. u. Hassan, R. Karhu, I. G. Ivanov, N. T. Son, J. R. Maze, T. Ohshima, Ö. O. Soykal, A. Gali, S.-Y. Lee, F. Kaiser, and J. Wrachtrup, High-fidelity spin and optical control of single silicon-vacancy centres in silicon carbide, *Nat. Commun.* **10**, 1954 (2019).

[24] E. Togan, Y. Chu, A. S. Trifonov, L. Jiang, J. Maze, L. Childress, M. V. G. Dutt, A. S. Sørensen, P. R. Hemmer, A. S. Zibrov, and M. D. Lukin, Quantum entanglement between an optical photon and a solid-state spin qubit, *Nature* **466**, 730 (2010).

[25] Ö. O. Soykal and T. L. Reinecke, Quantum metrology with a single spin-3/2 defect in silicon carbide, *Phys. Rev. B* **95**, 081405(R) (2017).

[26] D. Simin, V. A. Soltamov, A. V. Poshakinskiy, A. N. Anisimov, R. A. Babunts, D. O. Tolmachev, E. N. Mokhov, M. Trupke, S. A. Tarasenko, A. Sperlich, P. G. Baranov, V. Dyakonov, and G. V. Astakhov, All-Optical dc Nanotesla Magnetometry Using Silicon Vacancy Fine Structure in Isotopically Purified Silicon Carbide, *Phys. Rev. X* **6**, 031014 (2016).

[27] A. N. Anisimov, D. Simin, V. A. Soltamov, S. P. Lebedev, P. G. Baranov, G. V. Astakhov, and V. Dyakonov, Optical thermometry based on level anticrossing in silicon carbide, *Sci. Rep.* **6**, 33301 (2016).